





OUTAGE PERFORMANCE OF FULL-DUPLEX UNMANNED AERIAL VEHICLE-AIDED COOPERATIVE NON-ORTHOGONAL MULTIPLE ACCESS

Thanh Luan NGUYEN¹ , Thanh-Long NGUYEN² , Van Vinh NGUYEN³ ,
Tran Tin PHU⁴ 

¹ Faculty of Electronics Technology, Industrial University of Ho Chi Minh City,
12 Nguyen Van Bao, Ward 4, Go Vap District, 727000 Ho Chi Minh, Vietnam

² Faculty of Information Technology, Ho Chi Minh City University of Food Industry,
140 Le Trong Tan Street, Tay Thanh Ward, Tan Phu District, 760000 Ho Chi Minh City, Vietnam

³ Department of Information Assurance, FPT University, Hoa Lac Hi-tech Park,
Thang Long Avenue, Thach That District, 100000 Hanoi, Vietnam

⁴ Data Science Laboratory, Faculty of Information Technology, Ton Duc Thang University,
19 Nguyen Huu Tho street, Tan Phong ward, District 7, 756000 Ho Chi Minh City, Vietnam

nguyenthanhluan@iuh.edu.vn, longnt@hufi.edu.vn, vinhnv27@fe.edu.vn, phutrantin79@gmail.com

DOI: 10.15598/aeee.v21i1.4515

Article history: Received Mar 29, 2022; Revised Aug 30, 2022; Accepted Sep 16, 2022; Published Mar 31, 2023.
This is an open access article under the BY-CC license.

Abstract. *Unmanned Aerial Vehicles (UAVs) are envisioned to play a key role in the Sixth-Generation (6G) and Beyond Fifth-Generation (B5G) networks. Resolving spectrum constraints in UAV communications remains a critical issue. This article investigates Full-Duplex (FD) UAV-aided Non-Orthogonal Multiple Access (NOMA) to effectively utilise the scarce wireless spectrum. Specifically, exact closed-form formulas for the outage probability of FD UAV-aided NOMA have been developed. The results are validated using Monte Carlo simulation in 3GPP UMi conditions to provide practical guidelines for real-world deployment. In low transmission power regimes, the results also reveal that FD UAV-aided NOMA has a lower outage probability at the downlink Ground Users (GUs) than HD UAV-aided NOMA. At high transmit power regimes, FD UAV-aided NOMA is limited by residual SI at the UAV and interference from the UAV to the GUs. The numerical results also show that the transmission power at the UAV should be significantly lower than that at the Ground Base station (GB) to ensure low outages at the GUs.*

Keywords

Air-to-ground channel, full-duplex, NOMA, outage probability, unmanned aerial vehicle.

1. Introduction

The next Sixth-Generation (6G) wireless networks are envisioned to provide high security, high reliability, smart, and unlimited connection [1] and [2]. From self-directed vehicles to Unmanned Aerial Vehicles (UAVs), 6G technologies are expected to enable full-fledged architectures for connected devices and automated systems that demand reliable, low-latency, high-throughput, and energy-efficient services. UAVs, which include drones, play critical roles in beyond 5G and 6G networks due to their numerous applications in military and commercial applications such as low-latency communication, surveillance, navigation, air strikes, and remote control [1] and [4]. In [4], the Federal Aviation Administration (FAA) predicts that the number of commercial UAVs will reach 1.6 million by 2024 due to the ever-growing and ever-expanding deployment of UAVs.

Despite the advancement of 5G-related technologies like Non-Orthogonal Multiple Access (NOMA), spectrum scarcity continues to be a serious concern in UAV-aided networks [5], [6] and [7]. In the literature, conventional NOMA and Orthogonal Multiple Access (OMA) methods are expected to operate in Half-Duplex (HD) mode. As a result, orthogonal spectrum allocation is required for downlink users. Because the authorised frequency for UAV-aided communications is being utilised by multiple current wireless systems, effective resource allocation is essential to optimally utilise the wireless spectrum [8] and [9]. In this context, one promising approach is to develop Full-Duplex UAV-aided NOMA (FD UAV-aided NOMA) for wireless communication. When adopted for UAV-aided networks, FD UAV-aided NOMA allows uplink and/or downlink transmission of the ground devices and Ground Base station (GB) to occur within the same spectrum [10]. Although the use of FD and NOMA enhances spectrum efficiency [10], the self-interference of FD UAVs can be reduced using digital or analog interference cancellation architectures [11]. However, hardware impairments can lead to imperfect interference cancellation due to imperfect channel estimation, which eventually leaks out RSI and limits the performance of wireless networks [12] and [13]. On the other hand, FD UAV-aided NOMA communications are impeded by small scale fading, shadowing, and route loss, particularly in the urban environment, due to the continual presence of Line-of-Sight (LoS) blockage and relatively limited LoS to ground devices. Most studies do not investigate the interference from the FD UAV to the GUs because of the underlying network architectures [14] and [15], which can be undermined in specific networks, such as cellular networks with one cell-center GU near the GB and one cell-edge GU far away from the GB.

To this end, this paper investigates the performance of FD UAV-aided NOMA, where one GU has a direct link with the GB and is affected by the self-interference of the UAV. Specifically, the outage probability of FD UAV-aided NOMA communications is specifically compared to traditional Half-Duplex (HD) UAV-aided NOMA. The following are the paper's significant contributions:

- We apply air-to-ground channel models with the path loss model of 3GPP Urban Micro (UMi) in order to examine the performance of FD UAV-aided NOMA in practical scenarios.
- Exact closed-form expressions for the outage probability of the FD UAV-aided NOMA are presented and their correctness is validated by Monte Carlo simulation.

- At low transmit power regimes, it is shown that FD UAV-aided NOMA exhibits a lower outage probability than HD UAV-aided NOMA at the GB and at the downlink Ground devices (GUs). However, FD UAV-aided NOMA is limited by RSI at the UAV and at the GUs at high transmit power regimes.

The paper is organized as follows: First, we introduce the full-duplex UAV-aided NOMA system in Sec. 2. Specifically, we present the system model in Sec. 2.1, which includes the channel models for air-to-ground and ground-to-air communication. In addition, we also present the Signal-to-Noise-plus-Interference Ratios (SNIRs) and transmission models in Sec. 2.2. In Sec. 3, we discuss the likelihood of an outage. Then, in Sec. 4, we present our numerical findings and provide comments. Finally, we conclude the study in Sec. 5.

2. System Model

Consider a UAV-aided cooperative NOMA network consists of a full-duplex UAV that serves as an Aerial Relay (AR) in aerial cooperative networks, a Ground Base station (GB), and two Ground User equipment (GUs), namely GU_1 and GU_2 , as illustrated in Fig. 1. This communication situation might occur in a military battle scenario when one GU is not accessible to the terrestrial base stations and one GU must maintain a considerable distance to avoid being targeted. We assume that the direct link between the GB and the GU_2 is unavailable due to severe shadowing and large geographical separation, which is a reasonable assumption in urban and suburban areas where communication from one wireless node to another is frequently obstructed by high-rise buildings.

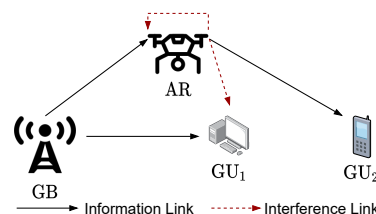


Fig. 1: Proposed full-duplex UAV-aided cooperative NOMA system.

2.1. Air-to-Ground Channel Model

We use the air-to-ground channel model presented in [16], [17] and [18] for Low Altitude Platforms

(LAP). It should be pointed out that LAPs, which are quasi-stationary, like helicopters, balloons, and quadcopters often have an altitude that is within the troposphere. As a results, LAPs are often significantly simpler to deploy due to their consistency with the broadband cellular. LAP technology is determined by the application, budget, and bandwidth, for example: Long Term Evolution (LTE)-A and Worldwide Interoperability for Microwave Access (WiMAX), as well as Global System for Mobile Communications (GSM) and P-25 networks [16]. The channel coefficients of the link from the AR to the GB and GUs can be presented in a unified form as:

$$h_{AR,X} = \epsilon_{AR,X} h_{AR,X}^{(1)} \sqrt{\eta_{AR,X}^{(1)} D_{AR,X}^{-\kappa^{(1)}}} + (1 - \epsilon_{AR,X}) h_{AR,X}^{(0)} \sqrt{\eta_{AR,X}^{(0)} D_{AR,X}^{-\kappa^{(0)}}}, \quad (1)$$

where $D_{AR,X}$, $X \in \{GB, GU_1, GU_2\}$, denotes the distance, $h_{AR,X}^{(1)}$, $\eta_{AR,X}^{(1)}$ and $h_{AR,X}^{(0)}$, $\eta_{AR,X}^{(0)}$ are the air-to-ground small-scale fading, the channel attenuation under the LoS and non-LoS (nLoS) condition, respectively; $\kappa^{(1)}$ and $\kappa^{(0)}$ are the path loss exponents, and $\epsilon_{AR,X} \in \{0, 1\}$ is the identity Random Variable (RV) depicting whether LoS is available over the AR - X link, where:

$$\mathbb{E}[\epsilon_{AR,X}] = \frac{1}{1 + \psi e^{-\omega(\theta_{AR,X} - \psi)}} \triangleq \xi_{AR,X}, \quad (2)$$

where ψ and ω are the environment-dependent coefficients, $\theta_{AR,X} = 180 \arctan(H_{AR}/R_{AR,X})/\pi$ denotes the polar angle of the AR with H_{AR} being the height of the AR, and $R_{AR,X}$ is the distance from X and the ground projection of the AR. The Cumulative Distribution Functions (CDFs) and the Probability Density Functions (PDFs) of $|h_{AR,X}^{(1)}|^2$ and $|h_{AR,X}^{(0)}|^2$ are given as:

$$F_{|h_{AR,X}^{(i)}|^2}(x) = 1 - e^{-m_{AR,X}^{(i)} x} \sum_{m=0}^{m_{AR,X}^{(i)}-1} \frac{(m_{AR,X}^{(i)})^m}{m!} x^m, \quad (3)$$

$$f_{|h_{AR,X}^{(i)}|^2}(x) = \frac{(m_{AR,X}^{(i)})^{m_{AR,X}^{(i)}}}{\Gamma(m_{AR,X}^{(i)})} x^{m_{AR,X}^{(i)}-1} e^{-m_{AR,X}^{(i)} x}, \quad (4)$$

respectively, where $m_{AR,X}^{(0)} = 1$ and $m_{AR,X}^{(1)} = m_{AR,X}$ with $m_{AR,X}$ being the shape factors of Gamma distributions and $\Gamma(x) = \int_0^\infty t^{x-1} e^{-t} dt$ is the Gamma function.

To this end, let us use α , β , ϕ and φ to represent the lower subscripts "AR,GB", "GB,GU₁", "AR,GU₁" and "AR,GU₂", respectively, for brevity. Accordingly, we consider the channel from GB to GU₁ experiencing Nakagami- m fading with shape μ_β

and mean λ_β , thus the corresponding channel power gain, i.e., $|h_\beta|^2$, follows Gamma distribution having the CDF:

$$F_{|h_\beta|^2}(x) = 1 - e^{-\frac{\mu_\beta x}{\lambda_\beta}} \sum_{m=0}^{\mu_\beta-1} \frac{(\frac{\mu_\beta}{\lambda_\beta})^m}{m!} x^m, \quad (5)$$

where $\lambda_\beta \triangleq \eta_\beta^{(1)} D_\beta^{-\kappa^{(1)}}$. Note that the Nakagami- m channel models are often utilized when the received signal at GU_1 is the aggregation of diffuse and specular scattering, or when the electric field is the sum of a strong component, which can be LoS, and many contributions with scattered components with small amplitude. Herein, the m parameter associates the amplitudes of the dominant LoS and scattering components in the Nakagami- m fading model, where Rayleigh fading is considered as a special case when $m = 1$ [26].

2.2. Transmission Model

According to the concept of downlink NOMA [6], [19] and [20], the GB transmits a superimposed coded mixture of information signals to the AR and the GUs. We consider imperfect Self-Interference (SI) cancellation at the AR and the GU_1 due to FD operation at the AR. In addition, AR only decodes GU_2 's information signal while treating GU_1 's signal as intra-user interference. Hence, the instantaneous SINR at the AR is formulated as:

$$\Gamma_{AR} = \frac{\Delta P_{GB} |h_\alpha|^2}{(1 - \Delta) P_{GB} |h_\alpha|^2 + P_{AR} |h_\chi|^2 + \sigma_{AR}^2}, \quad (6)$$

where $0 \leq \Delta \leq 1$ denotes the power allocation, P_{GB} and P_{AR} are the transmission powers of the GB and the AR, respectively, σ_{AR}^2 denotes the Additive White Gaussian Noise (AWGN) power at the AR, and $|h_\chi|^2$ specifies the power of the residual SI. We consider $|h_\chi|^2$ follows Gamma distribution with shape θ_χ and mean λ_χ , thus the PDF of $|h_\chi|^2$ is given by:

$$f_{|h_\chi|^2}(x) = \frac{(\frac{\theta_\chi}{\lambda_\chi})^{\theta_\chi}}{\Gamma(\theta_\chi)} x^{\theta_\chi-1} e^{-\frac{x\theta_\chi}{\lambda_\chi}}, \quad x > 0, \quad (7)$$

where λ_χ denotes the RSI level at the AR.

The GU_1 first decodes the interference signal from GU_2 , thus the corresponding achievable SINR is given by:

$$\Gamma_{GU_2 \rightarrow GU_1} = \frac{\Delta P_{GB} |h_\beta|^2}{(1 - \Delta) P_{GB} |h_\beta|^2 + P_{AR} |h_\phi|^2 + \sigma_{GU}^2}, \quad (8)$$

where $|h_\phi|^2$ denotes the SI power from the AR due to imperfect SI cancellation at the AR.

When GU_1 cancelled the GU_2 's interference signal via successive interference cancellation, GU_1 decodes

its own information signal, thus the corresponding SINR is given by:

$$\Gamma_{GU_1}^{e2e} = \frac{(1 - \Delta)P_{GB}|h_\beta|^2}{P_{AR}|h_\phi|^2 + \sigma_{GU}^2}. \quad (9)$$

Hence, the Signal-to-Noise Ratio (SNR) at GU_2 is given by:

$$\Gamma_{GU_2} = \frac{P_{AR}}{\sigma_{GU}^2}|h_\phi|^2. \quad (10)$$

The e2e SINR at GU_2 is the minimum achievable SINR for decoding its information signal, which is given by:

$$\Gamma_{GU_2}^{e2e} = \min[\Gamma_{GU_2 \rightarrow GU_1}, \Gamma_{AR}, \Gamma_{GU_2}]. \quad (11)$$

3. Outage Probability

In this section, we derive the exact closed-form expressions of the outage probability of the information signals of GU_1 and GU_2 . Outage probability, as a key performance metric for interference-limited systems, is defined as the probability that the achievable e2e SNR or SINR falls below a target threshold. The SINR threshold ensures that the GUs' minimal quality-of-service requirement is met. Mathematically speaking, the outage probability of GU_1 and GU_2 can be expressed in unified form as:

$$OP_{GU_j} \triangleq \Pr[\Gamma_{GU_j}^{e2e} < \tau_{GU_j}], \quad j = 1, 2, \quad (12)$$

where $\tau_{GU_j} = 2^{R_j} - 1$ denotes the target threshold of GU_j expressed in terms of R_j ((bits·s⁻¹)·Hz⁻¹), i.e., the target transmission rate.

Theorem 1. *The Outage Probability (OP) at the GU_1 can be expressed as:*

$$OP_{GU_1} = F_{\gamma_1}(c_1, c_2), \quad (13)$$

where $c_1 \triangleq \frac{\tau_{GU_1} \sigma_{GU}^2}{1 - \Delta} \frac{P_{GB}}{P_{AR}}$ and $c_2 \triangleq \frac{P_{AR}}{\sigma_{GU}^2}$.

Proof: Substituting Eq. (11) into Eq. (12) and utilizing some mathematical manipulations, we obtain:

$$\begin{aligned} OP_{GU_1} &= \Pr[\beta < c_1 c_2 \phi + c_1] = \\ &= \int_0^\infty F_\beta(c_1 c_2 x + c_1) f_\phi(x) dx. \end{aligned} \quad (14)$$

Substituting Eq. (4) and Eq. (5) into the above equation, the OP at the GU_1 becomes:

$$\begin{aligned} OP_{GU_1} &= 1 - \sum_i \int_0^\infty \sum_{j=0}^{\mu_\beta-1} \frac{(\frac{\mu_\beta}{\lambda_\beta})^j}{j!} (c_1 c_2 x + c_1)^j e^{-\frac{m_\phi^{(i)}}{\lambda_\phi^{(i)}} x} \\ &\quad \cdot e^{-(c_1 c_2 x + c_1) \frac{\mu_\beta}{\lambda_\beta} \frac{(\frac{m_\phi^{(i)}}{\lambda_\phi^{(i)}})^m}{\Gamma(m_\phi^{(i)})}} x^{m_\phi^{(i)}-1} dx, \end{aligned} \quad (15)$$

where $\lambda_\phi^{(i)} \triangleq \lambda_\chi \eta_\phi^{(i)} D_\phi^{-\kappa^{(i)}}$. By applying the binomial theorem to expand $(c_1 c_2 x + c_1)^j$ and utilizing the identity [21], we obtain $F_{\gamma_1}(c_1, c_2)$ in Eq. (20) at the top of the next page, where $A_{j_2}^{(i)} \triangleq \frac{j!(m_\phi^{(i)} + j_2 - 1)!}{(j - j_2)! j_2!}$. This completes the proof of Thm. 1.

Theorem 2. *The OP at the GU_2 can be expressed as:*

$$\begin{aligned} OP_{GU_2} &= 1 - (1 - F_{\gamma_2}(c_3, c_4)) \cdot \\ &\quad \cdot (1 - F_{\gamma_1}(c_5, c_6))(1 - F_\varphi(c_7)), \end{aligned} \quad (16)$$

where $c_4 \triangleq \frac{P_{AR}}{\sigma_{GU}^2}$, $c_3 \triangleq \frac{\tau_{GU_2}}{\Delta - \tau_{GU_2}(1 - \Delta)} \frac{P_{GB}}{\sigma_{GU}^2}$, $c_6 \triangleq \frac{P_{AR}}{\sigma_{AR}^2}$, $c_5 \triangleq \frac{\tau_{GU_2}}{\Delta - \tau_{GU_2}(1 - \Delta)} \frac{P_{GB}}{\sigma_{AR}^2}$ and $c_7 \triangleq \frac{\sigma_{GU}^2 \tau_{GU_2}}{P_{AR}}$.

Proof: By substituting Eq. (11) into Eq. (12), after some mathematical manipulations, the e2e OP at the GU_2 can be rewritten by:

$$\begin{aligned} OP_{GU_2} &= 1 - \Pr[\Gamma_{AR} \geq \tau_{GU_2}] \Pr[\Gamma_{GU_2} \geq \tau_{GU_2}] \cdot \\ &\quad \cdot \Pr[\Gamma_{GU_2 \rightarrow GU_1} \geq \tau_{GU_2}] = \\ &= 1 - \underbrace{\Pr[\beta \geq c_3(c_4 \phi + 1)]}_{1 - F_{\gamma_1}(c_3, c_4)} \underbrace{\Pr[\varphi > c_7]}_{1 - F_\varphi(c_7)} \cdot \\ &\quad \cdot \Pr[\alpha \geq c_5(c_6 \chi + 1)], \end{aligned} \quad (17)$$

where the second equality occurs as Γ_{AR} , $\Gamma_{GU_2 \rightarrow GU_1}$ and Γ_{GU_2} are independent. Accordingly, the second probability in the above equation can be derived as:

$$\begin{aligned} F_{\gamma_2}(c_5, c_6) &= 1 - \sum_i \sum_{j=0}^{m_\alpha^{(i)}-1} \int_0^\infty \frac{(\frac{m_\alpha^{(i)}}{\lambda_\alpha^{(i)}})^j}{j!} (c_5 c_6 x + c_5)^j \\ &\quad \cdot e^{-(c_5 c_6 x + c_5) \frac{m_\alpha^{(i)}}{\lambda_\alpha^{(i)}} \frac{(\frac{\theta_\chi}{\lambda_\chi})^{\theta_\chi}}{\Gamma(\theta_\chi)}} x^{\theta_\chi-1} e^{-x \frac{\theta_\chi}{\lambda_\chi}} dx, \end{aligned} \quad (18)$$

where $\lambda_\alpha^{(i)} \triangleq \eta_\alpha^{(i)} D_\alpha^{-\kappa^{(i)}}$. By applying the binomial theorem to expand $(c_5 c_6 x + c_5)^j$ and the utilizing the identity [21], we obtain $F_{\gamma_2}(c_5, c_6)$ in Eq. (20) at the top of the next page, where $B_{j_2}^{(i)} \triangleq \frac{j!(\theta_\chi + j_2 - 1)!}{j_2!(j - j_2)!}$. This completes the proof of Thm. 2.

$$\begin{aligned}
 F_{\gamma_1}(c_1, c_2) &= 1 - \\
 &+ \sum_i \xi_\phi^{(i)} \sum_{j=0}^{\mu_\beta-1} \frac{(\frac{\mu_\beta}{\lambda_\beta})^j}{j!} \frac{(\frac{m_\phi^{(i)}}{\lambda_\phi^{(i)}})^{m_\phi^{(i)}}}{\Gamma(m_\phi^{(i)})} \cdot \\
 &\cdot \sum_{j_2+j_1=j} A_{j_2}^{(i)} \frac{(c_2)^{j_2} (c_1)^{j_1} e^{-\frac{c_1 \mu_\beta}{\lambda_\beta}}}{\left(\frac{c_1 c_2 \mu_\beta}{\lambda_\beta} + \frac{m_\phi^{(i)}}{\lambda_\phi^{(i)}}\right)^{m_\phi^{(i)}+j_2}},
 \end{aligned} \quad (19)$$

$$\begin{aligned}
 F_{\gamma_2}(c_5, c_6) &= 1 - \\
 &+ \sum_i \xi_\alpha^{(i)} \sum_{j=0}^{m_\alpha^{(i)}-1} \frac{(\frac{m_\alpha^{(i)}}{\lambda_\alpha^{(i)}})^j}{j!} \frac{(\frac{\theta_\chi}{\lambda_\chi})^{\theta_\chi}}{\Gamma(\theta_\chi)} \cdot \\
 &\cdot \sum_{j_2+j_1=j} B_{j_2}^{(i)} \frac{(c_6)^{j_2} (c_5)^{j_1} e^{-\frac{c_5 m_\alpha^{(i)}}{\lambda_\alpha^{(i)}}}}{\left(\frac{c_5 c_6 m_\alpha^{(i)}}{\lambda_\alpha^{(i)}} + \frac{\theta_\chi}{\lambda_\chi}\right)^{\theta_\chi+j_2}},
 \end{aligned} \quad (20)$$

4. Results and Discussion

Monte Carlo simulations are performed in this subsection to validate the analyses performed in previous sections. Several systematic insights are also offered for practical use. In order to evaluate a FD UAV's potential in practice, we assume the UAV is placed at the height $H_{AR} = 20$ m, $R_\alpha = 60$ m and $R_\varphi = 30$ m. In addition, we apply the 3GPP UMi [22] and [23] and 5G UMi-Street Canyon [24] path loss models, thus $\psi = 9.61$ and $\omega = 0.16$ [25]. At the frequency band from 2 to 6 GHz and the distance range from 10 m to 2000 m, 3GPP UMi route loss models for LoS and nLoS transmission are presented as [22], [23] and [24] $PL_{LoS}(D) = 22 \log_{10}(D) + 28 + 20 \log_{10}(f_c)$ dB and $PL_{nLoS}(D) = 36.7 \log_{10}(D) + 22.7 + 26 \log_{10}(f_c)$ dB, respectively. In linear scale, these path loss models can be rewritten as:

$$PL_{LoS}(D) = 630.9573 \cdot D^{2.2} \cdot (f_c)^2, \quad (21)$$

$$PL_{nLoS}(D) = 186.2087 \cdot D^{3.67} \cdot (f_c)^{2.6}, \quad (22)$$

respectively, where f_c (GHz) denotes the carrier frequency. Using the aforementioned path loss models, the attenuation coefficients, measured in linear scale, are given as $\eta_{AR,X}^{(1)} \triangleq (630.9573 \cdot (f_c)^2)^{-1}$ and $\eta_{AR,X}^{(0)} \triangleq (186.2087 \cdot (f_c)^{2.6})^{-1}$ [22], [23] and [24]. The path loss exponents are given as $\kappa^{(1)} = 2.2$ and $\kappa^{(0)} = 3.67$ [22], [23] and [24]. We consider the noise power density at -134 dBm·Hz⁻¹ with the bandwidth of 10 MHz and the carrier frequency $f_c = 3$ GHz [17]. In addition, we assume that $\sigma_{GU_1}^2 = \sigma_{GU_2}^2 = \sigma_{AR}^2 = \sigma^2$. Moreover, the fading figures

of the information links are considered as $m_\alpha = 3$, $m_\varphi = 2$ and $\mu_\beta = 3$ and those of the interference links are $\theta_\chi = 3$ and $m_\phi = 2$.

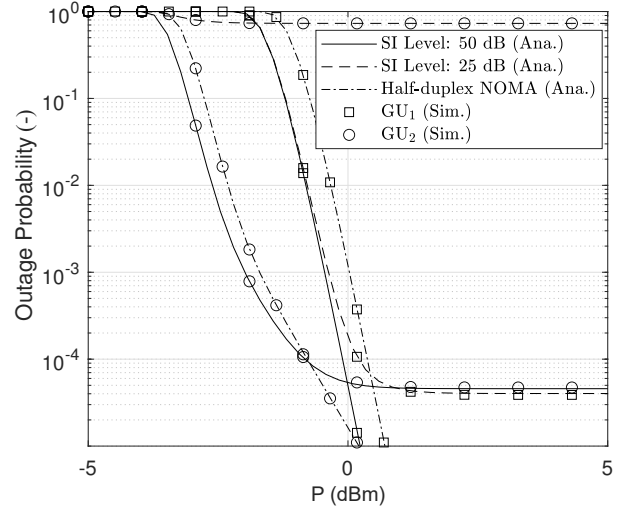


Fig. 2: Outage probability versus the transmission power $P_{AR} = P_{GB} = P$ (dBm) and RSI level.

In Fig. 2, we investigate the impact of transmission powers at the GB and AR with varying RSI levels. The simulation curves perfectly match the analytical curves, which validates the correctness of the analysis. In general, as P grows, the likelihood of an outage reduces, improving network dependability. In low transmission power regimes where $P(\text{dBm}) < 0$, the FD UAV-aided NOMA endures a lower outage rate than the HD UAV-aided NOMA. However, at high transmission power levels where $P(\text{dBm}) \geq 0$, the RSI at the UAV and interference from the UAV to the GUs limit the performance of FD UAV-aided NOMA and result in a higher outage probability than HD UAV-aided NOMA.

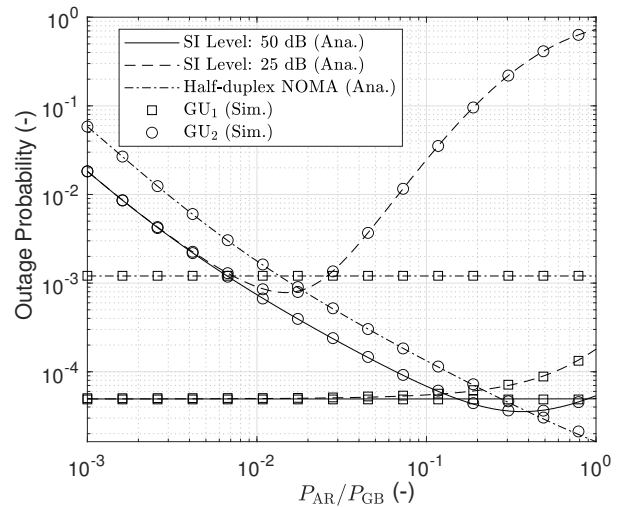


Fig. 3: Outage probability versus the ratio between the transmission power of AR and GB.

In Fig. 3, we examine the outage probability versus the ratio $\frac{P_{AR}}{P_{GB}}$ where $P_{GB}(\text{dBm}) = 0$. Again, the simulation curves fit precisely with the analytical curves, confirming the analysis's validity. As the considering ratio increases, so does the received SINR at GU_2 , lowering the outage probability of GU_2 until it reaches an optimal point. If the ratio $\frac{P_{AR}}{P_{GB}}$ is increased further, the RSI at the UAV and the interference from the UAV will grow significantly worse, reducing GU_2 's outage performance. When $\frac{P_{AR}}{P_{GB}}$ is small, e.g., less than 10^{-2} , the FD UAV-aided NOMA outperforms the HD UAV-aided NOMA. As a result, we recommend the UAV's transmission power to be substantially lower than that of the GB in order to achieve excellent transmission reliability.

5. Conclusion

The potential of FD UAV-aided NOMA for addressing spectrum shortages in UAV-aided networks is studied in this paper. For that purpose, closed-form outage probability equations for the FD UAV-aided NOMA networks are offered. At low transmit power regimes, the performance analysis at ground users revealed that FD UAV-aided NOMA had a lower outage probability than HD UAV-aided NOMA. In contrast, at high transmission power regimes, RSI at the UAV and interference to the downlink GUs limit the performance of FD UAV-aided NOMA. To enhance the performance of FD UAV-aided NOMA, the transmission power of the FD UAV should be much lower than that of the GB, otherwise high outages may occur at both GUs.

Author Contributions

T.-L.N. developed the system model. Both T.L.N. and T.T.P. performed the analytic calculations and performed the numerical simulations. All authors contributed to the final version of the manuscript. V.V.N. and T.-L.N. supervised the project.

References

- [1] SAAD, W., M. BENNIS and M. CHEN. A Vision of 6G Wireless Systems: Applications, Trends, Technologies, and Open Research Problems. *IEEE Network*. 2020, vol. 34, iss. 3, pp. 134–142. ISSN 1558-156X. DOI: 10.1109/MNET.001.1900287.
- [2] 6G – Connecting a cyber-physical world. In: *Ericsson* [online]. 2022. Available at: <https://www.ericsson.com/en/reports-and-papers/white-papers/a-research-outlook-towards-6g>.
- [3] MOZAFFARI, M., A. T. Z. KASGARI, W. SAAD, M. BENNIS and M. DEBBAH. Beyond 5G With UAVs: Foundations of a 3D Wireless Cellular Network. *IEEE Transactions on Wireless Communications*. 2019, vol. 18, iss. 1, pp. 357–372. ISSN 1558-2248. DOI: 10.1109/TWC.2018.2879940.
- [4] The Federal Aviation Administration (FAA) Aerospace Forecast Fiscal Years (FY) 2020-2040. In: *Federal Aviation Administration* [online]. 2020. Available at: <https://www.faa.gov/newsroom/federal-aviation-administration-faa-aerospace-forecast-fiscal-years-fy-2020-2040>.
- [5] HA, D.-H., T. T. DUY, P. N. SON, T. LE-TIEN and M. VOZNAK. Security-Reliability Trade-Off Analysis for Rateless Codes-Based Relaying Protocols Using NOMA, Cooperative Jamming and Partial Relay Selection. *IEEE Access*. 2021, vol. 9, pp. 131087–131108. ISSN 2169-3536. DOI: 10.1109/ACCESS.2021.3114343.
- [6] DAO, T.-T. T., S. Q. NGUYEN, H. NHUNG-NGUYEN, P. X. NGUYEN and Y.-H. KIM. Performance Evaluation of Downlink Multiple Users NOMA-Enable UAV-Aided Communication Systems Over Nakagami- m Fading Environments. *IEEE Access*. 2021, vol. 9, iss. 1, pp. 151641–151653. ISSN 2169-3536. DOI: 10.1109/ACCESS.2021.3124017.
- [7] ASWATHI, V. and A. V. BABU. Outage and Throughput Analysis of Full-Duplex Cooperative NOMA System With Energy Harvesting. *IEEE Transactions on Vehicular Technology*. 2021, vol. 70, iss. 11, pp. 11648–11664. ISSN 1939-9359. DOI: 10.1109/TVT.2021.3112596.
- [8] AZOULAY, R., Y. HADDAD and S. RECHES. Machine Learning Methods for UAV Flocks Management-A Survey. *IEEE Access*. 2021, vol. 9, iss. 1, pp. 139146–139175. ISSN 2169-3536. DOI: 10.1109/ACCESS.2021.3117451.
- [9] MASARACCHIA, A., Y. LI, K. K. NGUYEN, C. YIN, S. R. KHOSRAVIRAD, D. B. DA COSTA and T. Q. DUONG. UAV-Enabled Ultra-Reliable Low-Latency Communications for 6G: A Comprehensive Survey. *IEEE Access*. 2021, vol. 9, iss. 1, pp. 137338–137352. ISSN 2169-3536. DOI: 10.1109/ACCESS.2021.3117902.

- [10] BAEK, H. and J. LIM. Design of Future UAV-Relay Tactical Data Link for Reliable UAV Control and Situational Awareness. *IEEE Communications Magazine*. 2018, vol. 56, iss. 10, pp. 144–150. ISSN 1558-1896. DOI: 10.1109/MCOM.2018.1700259.
- [11] UR RAHMAN, S., G.-H. KIM, Y.-Z. CHO and A. KHAN. Positioning of UAVs for throughput maximization in software-defined disaster area UAV communication networks. *Journal of Communications and Networks*. 2018, vol. 20, iss. 5, pp. 452–463. ISSN 1976-5541. DOI: 10.1109/JCN.2018.000070.
- [12] TIN, P. T., T. N. NGUYEN, D.-H. TRAN, M. VOZNAK, V.-D. PHAN and S. CHATZINOTAS. Performance Enhancement for Full-Duplex Relaying with Time-Switching-Based SWIPT in Wireless Sensors Networks. *Sensors*. 2021, vol. 21, iss. 11, pp. 1–16. ISSN 1424-8220. DOI: 10.3390/s21113847.
- [13] NAM, P. M., P. T. TIN and M. TRAN. Intercept probability analysis in DF time switching full-duplex relaying network with impact of Co-channel interference at the eavesdropper. *Telecommunication Computing Electronics and Control*. 2020, vol. 18, iss. 5, pp. 2335–2340. ISSN 2302-9293. DOI: 10.12928/telkomnika.v18i5.13861.
- [14] LI, B., S. ZHAO, R. ZHANG and L. YANG. Full-Duplex UAV Relaying for Multiple User Pairs. *IEEE Internet of Things Journal*. 2021, vol. 8, iss. 6, pp. 4657–4667. ISSN 2327-4662. DOI: 10.1109/JIOT.2020.3027621.
- [15] MUCIN, D. P., D. P. M. OSORIO and E. E. B. OLIVO. Wireless-Powered Full-Duplex UAV Relay Networks Over FTR Channels. *IEEE Open Journal of the Communications Society*. 2021, vol. 2, iss. 1, pp. 2205–2218. ISSN 2644-125X. DOI: 10.1109/OJCOMS.2021.3113023.
- [16] AL- HOURANI, A., S. KANDEEPAN and S. LARDNER. Optimal LAP Altitude for Maximum Coverage. *IEEE Wireless Communications Letters*. 2014, vol. 3, iss. 6, pp. 569–572. ISSN 2162-2345. DOI: 10.1109/LWC.2014.2342736.
- [17] TANG, J., G. CHEN and J. P. COON. Secrecy Performance Analysis of Wireless Communications in the Presence of UAV Jammer and Randomly Located UAV Eavesdroppers. *IEEE Transactions on Information Forensics and Security*. 2019, vol. 14, iss. 11, pp. 3026–3041. ISSN 1556-6021. DOI: 10.1109/TIFS.2019.2912074.
- [18] KIM, M., S. KIM and J. LEE. Securing Communications With Friendly Unmanned Aerial Vehicle Jammers. *IEEE Transactions on Vehicular Technology*. 2021, vol. 70, iss. 2, pp. 1972–1977. ISSN 1939-9359. DOI: 10.1109/TVT.2021.3052503.
- [19] DUY, T. T., P. T. D. NGOC and P. T. TRAN. Performance Enhancement for Multihop Cognitive DF and AF Relaying Protocols under Joint Impact of Interference and Hardware Noises: NOMA for Primary Network and Best-Path Selection for Secondary Network. *Wireless Communications and Mobile Computing*. 2021, vol. 2021, iss. 1, pp. 1–15. ISSN 1530-8669. DOI: 10.1155/2021/8861725.
- [20] NGUYEN, B. C., T. M. HOANG, P. T. TRAN and T. N. NGUYEN. Outage probability of NOMA system with wireless power transfer at source and full-duplex relay. *AEU - International Journal of Electronics and Communications*. 2020, vol. 116, iss. 1, pp. 1–9. ISSN 1434-8411. DOI: 10.1016/j.aeue.2019.152957.
- [21] GRADSHTEYN, I. S. and I. M. RYZHIK. *Table of integrals, series, and products*. 8th ed. Cambridge: Academic Press, 2014. ISBN 978-0-12-384933-5.
- [22] 3GPP. Evolved universal terrestrial radio access (E-UTRA); further advancements for E-UTRA physical layer aspects. 2010.
- [23] BJORNSSON, E., O. OZDOGAN and E. G. LARSSON. Intelligent Reflecting Surface Versus Decode-and-Forward: How Large Surfaces are Needed to Beat Relaying? *IEEE Wireless Communications Letters*. 2020, vol. 9, iss. 2, pp. 244–248. ISSN 2162-2345. DOI: 10.1109/LWC.2019.2950624.
- [24] RAPPAPORT, T. S., Y. XING, G. R. MACCARTNEY, A. F. MOLISCH, E. MELLIOS and J. ZHANG. Overview of Millimeter Wave Communications for Fifth-Generation (5G) Wireless Networks—With a Focus on Propagation Models. *IEEE Transactions on Antennas and Propagation*. 2017, vol. 65, iss. 12, pp. 6213–6230. ISSN 1558-2221. DOI: 10.1109/TAP.2017.2734243.
- [25] KHAN, S. K., U. NASEEM, A. SATTAR, N. WAHEED, A. MIR, A. QAZI and M. ISMAIL. UAV-aided 5G Network in Suburban, Urban, Dense Urban, and High-rise Urban Environments. In: *2020 IEEE 19th International Symposium on Network Computing and Applications (NCA)*. Cambridge: IEEE, 2020, pp. 1–4. ISBN 978-1-72818-326-8. DOI: 10.1109/NCA51143.2020.9306710.

- [26] DERSCH, U. and R. J. RUEGG. Simulations of the time and frequency selective outdoor mobile radio channel. *IEEE Transactions on Vehicular Technology*. 1993, vol. 42, iss. 3, pp. 338–344. ISSN 1939-9359. DOI: 10.1109/25.231886.

About Authors

Thanh Luan NGUYEN received the B.S. degree (Valedictorian) from the Ho Chi Minh City University of Technology and Education, Vietnam, in 2016. He is currently a Research Assistant with the Faculty of Electronics Technology, Industrial University of Ho Chi Minh City (IUH). His research interests include NOMA, stochastic geometry, generalized fading channels, and other emerging wireless technologies.

Thanh-Long NGUYEN (corresponding author) is currently the Vice Dean of Faculty of Information Technology, Ho Chi Minh City University of Food Industry, Ho Chi Minh City, Vietnam. He was born on July 15, 1970 in Binh Thuan Province. He graduated in information technology in 2003 from University of Science, Ho Chi Minh City, Vietnam. In 2011, he received Master degree in Computer Science from Hue University, Thua Thien-Hue Province, Vietnam. He has taught in the information technology at Ho Chi Minh City University of Food Industry (former Junior College of Food Industry) since 1999. In 2021, he graduated

and received the Ph.D diploma at VSB-Technical University of Ostrava in the Czech Republic. He was actively involved in three research projects at Ho Chi Minh city University of Food Industry, one of which is a member and the other two are principal investigator. His research interests include Applied Informatics, Knowledge Discovery, Data Mining, Information and Communications Technology.

Van Vinh NGUYEN received the B.E. degree in Computer Science from Nha Trang University, Vietnam, in 2008. In 2015, he received a Master's degree in Computer Science from University of Transport and Communications, Vietnam. He is currently a lecturer at the Department of Information Assurance (IA), FPT University Hanoi, Ho Chi Minh City, Vietnam. His research interests are wireless communication in 5G, networking, cybersecurity, physical layer security and NOMA.

Tran Tin PHU received the Bachelor's degree (2002) and Master's degree (2008) from Ho Chi Minh City University of Science. He is currently a lecturer at the Faculty of Information Technology, Ton Duc Thang University, Ho Chi Minh City, Vietnam. In 2019, he received the Ph.D. degree in Faculty of Electrical Engineering and Computer Science, VSB-Technical University of Ostrava, Czech Republic. His major research interests are wireless communication in 5G, energy harvesting, performance of cognitive radio, physical layer security and NOMA.